



# Pickering emulsion enhanced interfacial catalysis under Taylor flow in a microchannel reactor

Hongye Li<sup>a</sup>, Xunli Zhang<sup>b</sup>, Qingqiang Wang<sup>a,\*</sup>, Nan Jin<sup>a</sup>, Haisheng Wei<sup>a</sup>, Yuchao Zhao<sup>a,\*</sup>

<sup>a</sup> Shandong Key Laboratory for Chemical Engineering and Processing, College of Chemistry & Chemical Engineering, Yantai University, Yantai 264005, China

<sup>b</sup> School of Engineering & Institute for Life Sciences, University of Southampton, Southampton SO17 1BJ, UK



## ARTICLE INFO

### Keywords:

Microchannel  
Microreactor  
Multiphase flow  
Mass transfer  
Pickering emulsion  
Oxidation

## ABSTRACT

There are still technical challenges associated with surface fouling and clogging in microchannels when conducting multiphase catalytic reactions involving solid particles. In this study, a Pickering emulsion was employed to enhance the oxidation of benzyl alcohol (BNOH) catalyzed by Pd/SiO<sub>2</sub> nanoparticles under Taylor flow in a microchannel reactor. The reaction characteristics of benzyl alcohol/water Pickering emulsion in a microchannel reactor were studied experimentally. The characteristic results showed that the O/W Pickering emulsion system was superior to the W/O Pickering emulsion system for the catalytic oxidation reaction. The influences of a wide range of operational variables were characterized on the conversion of reactants and the selectivity of the desired product. The optimized reaction conditions included: reaction temperature 403 K, CB 5 wt%, O<sub>2</sub>/BNOH (mol/mol) 0.76 and tube length 8 m. Under the optimal operating conditions, the conversion of BNOH and the selectivity of benzaldehyde were found to be 86.53% and 99.79%, respectively. In addition, the interfacial transport-reaction mechanism in Pickering emulsions under Taylor flow in microchannels was proposed from the perspective of multiphase mass transfer. This development provided significant insights and guiding for effectively performing multiphase catalytic reactions involving solid catalyst particles in microchannel reactors.

## 1. Introduction

Over the past few decades, the microchannel reactor technology has advanced considerably, exhibiting remarkable performance in chemical process intensification [1–3]. Compared to conventional batch or semi-batch reactors on a macroscale, microchannel reactors possess numerous advantages, including a considerable specific surface area, rapid heat and mass transfer rates, minimal back-mixing (resulting in a plug flow reactor), intrinsic process safety, and scalability through numbering-up [4–11]. Despite these advantages, there are still some key challenges for wider applications of multiphase reactions involving gas–liquid–solid or solid–liquid systems, that are mainly associated with the significant fouling and clogging with microchannels caused by solid particulate materials [12]. This is of direct relevance to heterogeneous solid catalytic reaction processes which occupy a very large proportion of reactions in the chemical industry [13,14]. Therefore, enormous efforts have been made to improve continuous multiphase flow reaction systems involving solid catalyst particles in microchannels [15].

One of the most commonly employed strategies to solve the packing problem of solid catalyst materials is to have the solid particles adhered

or coated to the inner wall of the microchannel [16,17]. Although the coated thin film is well suited for fast reactions due to the enhanced internal diffusion rate, there are some inherent drawbacks, such as the limited amount of catalyst loaded, easier washing away of the catalytic active components, and the difficulty of regenerating deactivated catalysts [18,19]. An alternative approach is to pack the microchannel with the solid catalyst particles having a diameter in the range of micrometers. This can be considered as a micro-packed bed reactor [20–22] having advantages such as simplicity for catalysts replacing and good catalytic performance. However, the drawback of this type of micro-reactor includes high pressure drops, severe wall effects, poor uniformity of catalytic bed and reproducibility [23–25]. To address these issues, the concept of micro-suspended reactor has been recently proposed [19,26], which also overcomes the problem of catalyst loading and transportation, opening up a new direction for handling solid particulate catalysts in microchannel reactors. However, the process is linked to several technical challenges, such as adhesion phenomena. This occurs when the catalyst particles come into contact with the channel wall, potentially leading to the obstruction of the channel in the most severe circumstances. This is largely attributed to the size of solid catalyst particles, which typically range in the nanometer scale and

\* Corresponding authors.

E-mail addresses: [wangqq3033@ytu.edu.cn](mailto:wangqq3033@ytu.edu.cn) (Q. Wang), [yczhao@ytu.edu.cn](mailto:yczhao@ytu.edu.cn) (Y. Zhao).

**Nomenclature**

|                       |  |                    |   |
|-----------------------|--|--------------------|---|
| $CB$                  | mass ratio of catalyst to benzyl alcohol     | $M_{\text{Water}}$ | molar mass of water phase, g/cm <sup>3</sup>  |
| $Ca$                  | capillary number                             | $m_p$              | total mass of catalyst particle, g  |
| $U$                   | velocity, $\mu\text{m}\cdot\text{s}^{-1}$    | $\theta$           | three-phase contact angle, °  |
| $\mu_C$               | continuous phase viscosity, mPa·s            | $\tau$             | coverage degree   |
| $\sigma_{12}$         | oil–water phases interfacial tension, mN/m   | $D$                | microchannel diameter, μm   |
| $\varepsilon$         | extension rate, s <sup>-1</sup>              | $D_p$              | average diameter of catalyst particle, μm   |
| $R$                   | maximum radius of droplets not broken, μm    | $D_D$              | Pickering emulsion droplet diameter, μm   |
| $\Delta V$            | volume variation of a single droplet, mL     | $D_B$              | bubble diameter, μm   |
| $V_{\text{Oil}}$      | oil phase volume, mL                         | $L_B$              | bubble length, μm   |
| $V_{\text{Water}}$    | water phase volume, mL                       | $L_S$              | liquid plug length, μm  |
| $V_d$                 | dispersed phase droplet volume, mL           | $N$                | number of droplets  |
| $V_{d0}$              | initial dispersed phase droplet volume, mL   | $S$                | surface area of the single bubble, cm <sup>2</sup>                                    |
| $V$                   | single bubble volume, mL                     | $S_{\text{OW}}$    | oil–water interface area, cm <sup>2</sup>   |
| $\rho_{\text{Oil}}$   | oil phase density, g/cm <sup>3</sup>         | $S_A$              | the specific surface area corresponding to unit volume of oil phase, cm <sup>-1</sup> |
| $\rho_{\text{Water}}$ | water phase density, g/cm <sup>3</sup>       | $x$                | reaction conversion rate  |
| $\rho_p$              | catalyst particle density, g/cm <sup>3</sup> | $t$                | resident time, s  |
| $M_{\text{Oil}}$      | molar mass of oil phase, g/cm <sup>3</sup>   | $Q$                | total volume flow rate, μL/min  |
|                       |  | $V_m$              | the reactor volume, mL  |

possess significant surface energy [27,28]. Furthermore, most of catalytic reactions require effective heat transfer in time through the wall of the microchannel in order to minimize the possible heat transfer lags behind which can potentially lead to a surge with the temperature around the catalyst particles resulting in increased side reactions.

Pickering emulsion is a novel colloidal system proposed recently, featured by its stabilization mechanism by using double-hydrophilicity solid particles that are located at the oil–water interface (e.g., see Fig. 1) [29]. Owing to its unique properties (e.g., the irreversible adsorption of solid particles in an oil–water interface), Pickering emulsion provides a promising platform to address the above-mentioned existing problems of micro-suspension bed reactors. Compared the conventional emulsions stabilized by organic chemical surfactants, Pickering emulsion has demonstrated significant performance especially for the resistance of droplets coalescence largely due to a dense layer of solid particles [30,31]. This is particularly beneficial for the emulsification of oil/water systems requiring high stability requirements, partial oil/water miscibility, and low interfacial tension between the oil and water phases. Within a microchannel, the surface energy of solid particles is largely released at the liquid–solid interface, which reduces the possibility of solid particles directly contacting the channel wall thus alleviating or eliminating the wall surface fouling [32].

In the Pickering emulsion the intimate contact between the aqueous

phase and the solid stabilizing particles is also beneficial for heat transfer, e.g. to effectively remove or input heat of/into the reaction system. Therefore, the reaction temperature can be accurately controlled, thus enhance the selectivity of the reaction. In addition, the Pickering emulsion system has a large oil–water interface area, enabling higher extraction rates to extract the target product from the reaction phase thus also contributing to the improvement of reaction selectivity [33]. However, in-depth understanding is still being sought about the heat/mass transfer in Pickering emulsions and associated heterogeneous catalytic reactions in microchannel, whilst overall there have been very limited studies on the interfacial catalysis in Pickering emulsions within microchannel reactors [34].

Based on our previous research on Pickering emulsions stabilized by SiO<sub>2</sub> nanoparticles and the hydrodynamics of Pickering emulsion within microreactors [35,36], the present study aimed to develop a regulation strategy for the interfacial catalysis in Pickering emulsions in a micro-channel reactor, and gain insights into the mechanism of enhanced heterogeneous catalysis coupled with interfacial mass transfer. The oxidation of benzyl alcohol by O<sub>2</sub> was selected as a model reaction in the oil-in-water (O/W) Pickering emulsion system in a microchannel reactor under Taylor flow, where Pd/SiO<sub>2</sub> nanoparticles acted as both solid catalysts and Pickering emulsion stabilizers. Using the benzyl alcohol–water Pickering emulsion, the effects of a range of process parameters

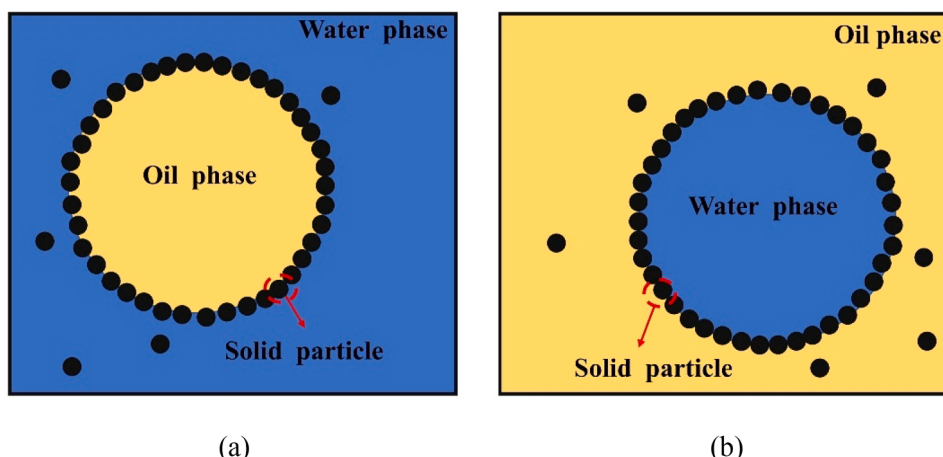


Fig. 1. Schematic diagrams of (a) O/W and (b) W/O Pickering emulsion.

on the reaction conversion rate and target product yield were characterized. Furthermore, the interfacial catalytic mechanism based Pickering emulsion was investigated from the perspective of mass transfer across multiphase interfaces in microchannels.

## 2. Experimental

### 2.1. Chemicals

$\text{SiO}_2$  nanoparticles (10 nm) were purchased from Shanghai Yuanjiang Chemical Co., Ltd, China. Palladium acetate (99.9%), 3-aminopropyltriethoxysilane (98%), cyclohexylmethyldimethoxysilane (97%), benzaldehyde ( $\geq 99.5\%$ ), benzoic acid ( $\geq 99.9\%$ ) and benzoic acid ( $\geq 99.9\%$ ) were obtained from Aladdin Industrial Co., Ltd, China. Benzyl alcohol ( $\geq 99.0\%$ ) was purchased from Sinopharm Chemical Reagent Co., Ltd, China. All chemicals and reagents were utilized without additional treatment or purification.

### 2.2. Preparation of materials and Pickering emulsions

Firstly, the  $\text{SiO}_2$  nanoparticles with interfacial activity were prepared with a method adapted from our previous research [35]. Briefly, to obtain the amphiphilic  $\text{SiO}_2$  nanoparticles, 1 g of  $\text{SiO}_2$ , a certain quantity of 3-aminopropyltriethoxysilane, cyclohexylmethyldimethoxysilane, and 30 mL of toluene were sequentially added into a homogeneous batch reactor. The reactor consisted of a rotating device (10 Hz) containing eight stainless steel vessels and a forced convection oven. The reaction temperature and time for the preparation of amphiphilic  $\text{SiO}_2$  nanoparticles were set to 130 °C and 12 h, respectively.

The Pd/ $\text{SiO}_2$  catalyst was then prepared by a conventional impregnation method [37]. Palladium acetate was dissolved in toluene to form a metal precursor solution with the concentration of 2.1 mg/mL. The prepared  $\text{SiO}_2$  nanoparticles and the metal precursor solution were added into the round-bottom flask, and the solution was stirred at room temperature for 5 h. Then, the Pd-containing solid particles were reduced with  $\text{NaBH}_4$  while stirred at room temperature for further 5 h. The suspended solid particles in the reactor were separated by centrifuge and washed with anhydrous ethanol. Whereafter, the obtained Pd/ $\text{SiO}_2$  particles were dried under vacuum at 40 °C for 12 h.

Prior to adding the dispersed phase (water or benzyl alcohol), a homogenous suspension with the mixtures of Pd/ $\text{SiO}_2$  and the continuous phase (benzyl alcohol or water) was prepared through ultrasonic treatment. Finally, Pickering emulsion was prepared with the help of a vortex mixer (IKA T25 digital Ultra Turrax, S25N-18G, German).

### 2.3. Characterization

The contact angle of the solid nanoparticles was measured by an optical tensiometer (JC2000, Shanghai Zhongchen Digital Technology Equipment Co., Ltd.). The morphology and microstructure of the emulsion droplets were captured using an inverted microscope (Olympus IX73P2F, Japan) equipped with a high-speed digital camera (Phantom Miro R311, USA). The flow state of Pickering emulsion- $\text{O}_2$  two-phase system was recorded using a stereo microscope (Olympus SZX16, Japan) equipped with a high-speed camera. By processing the digital images captured by ImageJ, the length of the Pickering emulsion droplets and the distance between two liquid plugs or two bubbles were determined.

### 2.4. Experimental setup and analysis

Fig. 2 illustrates the experimental setup for the liquid phase oxidation of benzyl alcohol under Taylor flow in the microchannel. Pickering emulsion and  $\text{O}_2$  are injected into the FEP preheating tube (i.d. 500  $\mu\text{m}$ , IDEX Health& Science) by a precision syringe pump (Harvard 11 ELITE Single, USA) and a high-pressure syringe pump (Longer pump LSP01-1BH, CHINA), respectively. The two phases were mixed at the PTFE T-mixer (i.d. 500  $\mu\text{m}$ , IDEX Health & Science). The gas–liquid mixture flowed down the FEP reaction tube (i.d. 500  $\mu\text{m}$ , 760  $\mu\text{m}$ , 1000  $\mu\text{m}$ , or 1590  $\mu\text{m}$ ; length 0.5–10 m; Nichias Corporation), where the two-phase fluids flowed in the slug flow pattern. The FEP reaction tube was heated through an oil bath. In this experiment, the inner diameter of the microchannel reactor was about 0.5 mm, the heat transport rate was very fast. Therefore, the set temperature of the oil bath was considered as the same as the reaction system. Additionally, in the Pickering system, catalytic particles were always in close contact with the aqueous phase, effectively reducing thermal lag. Except for special requirements, all reaction processes were performed under the pressure of 100 psi in the study. The residence time ( $t$ ) can be calculated by the following equation:

$$t = \frac{V_m}{Q} \quad (1)$$

where  $V_m$  is the reactor volume,  $Q$  is the total volume flow rate of gas–liquid phase. To mitigate the impact of unsteady state conditions on reaction performance, the double residence time was implemented for at least one run prior to collecting the sample. The reaction solution at the outlet of the microchannel reactor was collected in a gas–liquid separator prior to further chemical analysis. Each experiment was repeated independently more than three times to ensure data accuracy. All

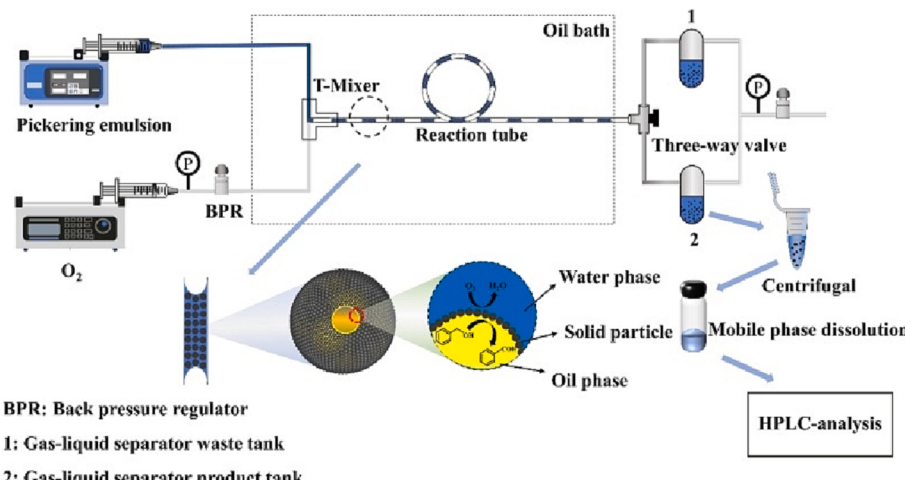


Fig. 2. Schematic of experimental setup for Pickering emulsion-catalyzed oxidation of benzyl alcohol in a microchannel reactor.

conversion and selectivity data are reproducible within an experimental error of  $\pm 3\%$ .

Chemical analysis was carried out with HPLC (Waters e2695, USA) equipped with an UV-visible absorbance detector (Waters 2998PDA, USA) and a C18 column (Agilent Eclipse Plus, USA) where all liquid samples were dissolved in the mobile phase. The chromatographic column temperature was 308 K, and the mobile phase with a flow rate of  $1.0 \text{ mL}\cdot\text{min}^{-1}$  was made of methanol (60 vol%) + water (40 vol%). The composition of samples was quantified using an external standard method. The total molar concentration of benzyl alcohol ( $c_{\text{total BNOH}}$ ) in the reaction solution was determined by the peak area normalization. The conversion of benzyl alcohol ( $x_{\text{BNOH}}$ ) was calculated using the following equation:

$$x_{\text{BNOH}} = \left( 1 - \frac{c_{\text{BNOH}}}{c_{\text{total BNOH}}} \right) \times 100\% \quad (2)$$

where  $c_{\text{BNOH}}$  is the molar concentration of benzyl alcohol in the sample.

The selectivity of benzaldehyde ( $S_{\text{Benzaldehyde}}$ ) was expressed by:

$$S_{\text{Benzaldehyde}} = \left( \frac{c_{\text{Benzaldehyde}}}{c_{\text{total BNOH}} - c_{\text{BNOH}}} \right) \times 100\% \quad (3)$$

where  $c_{\text{Benzaldehyde}}$  denotes the molar concentration of benzaldehyde in the sample.

The yield of product benzaldehyde ( $Y$ ) was obtained by the following equation:

$$Y = S_{\text{Benzaldehyde}} \times x_{\text{BNOH}} \quad (4)$$

The catalyst to benzyl alcohol mass ratio ( $CB$ ) was defined as:

$$CB = \frac{m_{\text{catalyst}}}{m_{\text{BNOH}}} \times 100\% \quad (5)$$

where  $m_{\text{catalyst}}$  is the mass of catalyst solid particles added, and  $m_{\text{BNOH}}$  is the mass of benzene methanol.

### 3. Results and discussion

#### 3.1. Properties of Pickering emulsions

**3.1.1. Characterization of Pickering emulsions**

The surface hydrophobicity of the nanoparticles was characterized by measuring the contact angle of water droplets on the surface of the flake, which was made from the raw  $\text{SiO}_2$  nanoparticles, modified  $\text{SiO}_2$  nanoparticles, or Pd/ $\text{SiO}_2$  nanoparticles. The contact angles of these three types of nanoparticles were measured to be  $14.0^\circ$ ,  $18.8^\circ$  and  $19.6^\circ$  (Fig. 3). As the contact angle of solid nanoparticles was mainly influenced by the adsorption of oil and water phases on their surfaces, with the increase of the oil phase polarity, the interfacial tension between oil phase and water phase decreased, thus the contact angle of water phase on the solid surface increased [38,39]. Based on the above analysis, the contact angle and wettability of the nanoparticles were regulated by concurrently grafting both hydrophilic and hydrophobic organic functional groups because benzyl alcohol, as a polar oil phase, tended to form W/O-type emulsions.

To examine the emulsion morphology and stability with different

solid-liquid composition, the added amount of catalyst solid particles and oil-to-water ratio were varied while the droplet diameter and stability of the emulsion were characterized. The results are shown in Fig. 4. It was found that there was a reduction in the emulsion droplet diameter when the added amount of catalyst solid particles increased. It was likely caused by the fact that the desorption energy of the solid particles desorbing from the biphasic interface was higher (typically by several times) than the thermodynamic energy. Therefore, an increase in the particle concentration improved the degree of surface coverage and prevented the coalescence between the emulsion droplets [40].

The effects of varying oil-to-water ratio were found to be in line with that observed in our earlier studies [35]. The volume change of continuous phase had little impact on the stability and size of the emulsion droplets [41], whilst in contrast the reduction of the dispersed phase volume increased the interface film densities of solid particles. Further, when the volume of the dispersed phase was reduced to a threshold level, the surplus solid particles started to break through the barrier of the interfacial adsorption energy thus enter into the continuous phase [42]. With a given amount of solid particles, therefore, the decrease in the volume of the dispersed phase had the same effect on the diameter of emulsion droplets as the increase in the solid particles did.

The stability of the Pickering emulsions was evaluated by determining capillary number ( $Ca$ ) [43], in a similar way used for conventional emulsions.

$$Ca = \frac{U\mu_C}{\sigma_{12}} = \frac{(\varepsilon R\mu_C)}{\sigma_{12}} \quad (6)$$

where  $U$  is the velocity,  $\mu_C$  is viscosity of the continuous phase,  $\sigma_{12}$  is the interfacial tension between the oil–water phases,  $\varepsilon$  is the extension rate, and  $R$  is the maximum radius of the drops that not broken, respectively.

According to Eq. (6),  $Ca$  is proportional to the size of the dispersed phase droplet,  $R$ . It was also found that, when  $Ca$  exceeded a critical value, the stability of the emulsion was destroyed and the droplets of the dispersed phase coalesced [44]. In contrast, by decreasing the diameter of the dispersed phase droplet the stability of the emulsion can be increased [45], realized by either adding more solid particles or reducing the volume of the dispersed phase.

#### 3.1.2. Effects of O/W and W/O Pickering emulsions

Depending on the continuous phase selected, Pickering emulsions can be generated in the form of either O/W or W/O configuration. Considering the effects of heat and mass transfer across phases on the reaction conversion and selectivity, the selection of a suitable emulsion type is crucial to match and enhance the multiphase reaction performance. For the oxidation of benzyl alcohol, the effects of both O/W and W/O emulsions were initially characterized on the interfacial catalytic reaction process in the Pickering emulsion system. Based on previous studies [46,47] on a similar reaction system, i.e. the Ru/CNT-TiO<sub>2</sub>-catalyzed oxidation of benzyl alcohol, two models of O/W and W/O emulsions were developed mapping the pathways for both reaction and mass transfer in the Pickering emulsion multiphase flow system, as schematically shown in Fig. 5.

The reaction process can take place in both types of emulsions though through different pathways (Fig. 5). On the one hand, oxygen molecules enter into the continuous phase (either aqueous or oil phase)

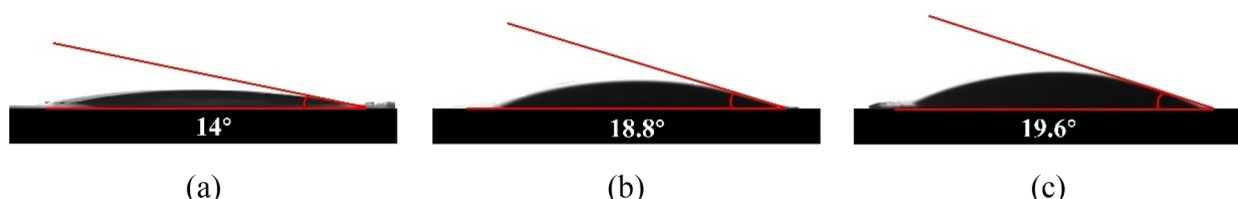


Fig. 3. Contact angles of different nanoparticles. (a) Raw  $\text{SiO}_2$ , (b) modified  $\text{SiO}_2$ , and (c) Pd/ $\text{SiO}_2$ .

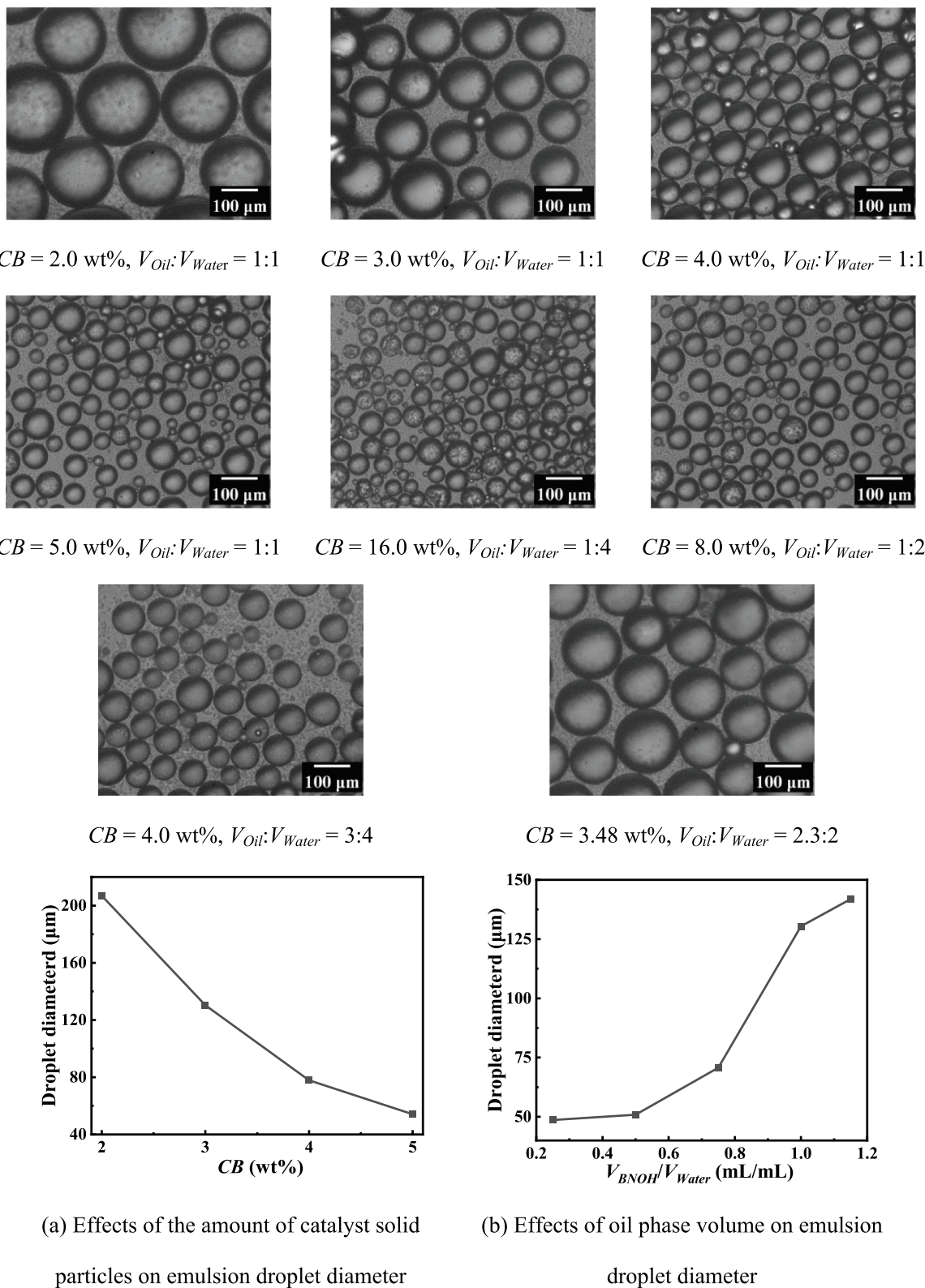
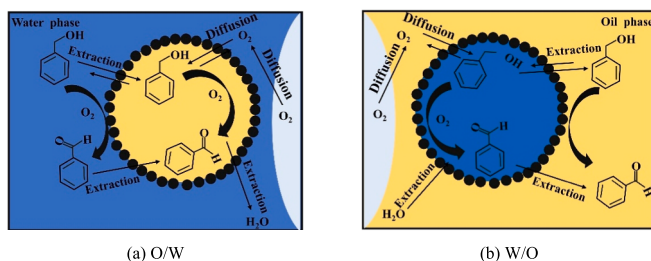


Fig. 4. Microscopic images of Pickering emulsion droplets and mean droplet diameter changes under different conditions.

and subsequently reach the oil–water interface by diffusion. On the other hand, the benzyl alcohol spontaneously diffuses towards the surface of solid catalytic particles distributed at the oil–water interface, where the catalyzed oxidation reaction of benzyl alcohol occurs and the product benzaldehyde is generated. As the solubility of benzaldehyde in

water is different from that in oil, the benzaldehyde generated is more favorably extracted into the oil phase [33].

It was noted that in the W/O emulsion system, the diameter of the dispersed aqueous droplets increased along the microchannel with the increase of reactant conversion. That was believed to be resulted from



**Fig. 5.** Physical models showing pathways of mass transfer coupled with oxidation reaction of benzyl alcohol in (a) O/W and (b) W/O Pickering emulsion systems under Taylor flow.

the additional water generated from the reaction which was subsequently extracted into the existing water droplet (Fig. 5(b)). To further quantify the water droplet change in the W/O emulsion system along with chemical reaction, a mathematical model was proposed to express the volume variation of a single droplet.

$$\Delta V = \frac{V_{Oil}\rho_{Oil}M_{Water}x}{M_{Oil}\rho_{Water}N} \quad (7)$$

where  $V$  and  $\rho$  are the volume and density of a substance (either water or oil), respectively;  $M$  is the molar mass of a substance;  $x$  and  $N$  are the conversion of benzyl alcohol and the number of droplets, respectively.

As found in previous studies [35], the coverage degree ( $\tau$ ) on the surface of the emulsion droplets is a relatively ideal evaluation index for the stability of Pickering emulsion, and index  $\tau$  can be expressed by the following equation:

$$\tau = \frac{m_p D_p \sin^2 \theta}{4 \rho_p D_p V_d} \quad (8)$$

$V_d$  is obtained by,

$$V_d = V_{d0} + \Delta V \quad (9)$$

where the subscripts  $d$  and  $p$  are the dispersed phase droplets and catalyst particles, respectively;  $m$  and  $D$  are the total mass and the average diameter of catalyst particles;  $\theta$  is the contact angle between oil and water phases.

Combined with Eqs. (7)–(9), the following equation can be derived.

$$\tau = \sqrt[3]{\frac{1}{(M_{Oil}\rho_{Water}NV_{d0} + V_{Oil}\rho_{Oil}M_{Water}x)^2}} H \quad (10)$$

where  $H$  is given by,

$$H = \sqrt[3]{\frac{6(M_{Oil}\rho_{Water}N)^2}{\pi} \frac{m_p \sin^2 \theta}{\rho_p D_p}} \quad (11)$$

It can be clearly see from Eq. (10) that as the conversion rate increases, both the particle coverage degree ( $\tau$ ) on the surface of W/O emulsion droplets and the stability of the emulsion decrease. This may lead to the agglomeration of droplets in the process of internal circulation flow. At the same time, the specific phase interface subsequently decreases, which can result in the reduction of benzaldehyde yield in the W/O emulsion system, even demulsification and channel clogging.

Based on the above analysis, the increase in conversion rate has little effect on the droplet size in the O/W emulsion system because the generated water is extracted into the continuous phase (Fig. 5(a)). The effects of products on the dispersed droplets could be ignored [35]. That explained the observation of the O/W emulsion system where there was little change in the oil droplet size. Therefore, the stability of O/W Pickering emulsions can be considered significantly more beneficial than that of W/O Pickering emulsions for the catalytic reaction process and, in turn, the yield of product benzaldehyde.

To verify the above hypothetical models, experiments were carried out to measure the yield of product benzaldehyde in both O/W and W/O Pickering emulsions. The results are shown in Fig. 6. As can be clearly seen from the figure, while both yields of benzaldehyde increased with the increase of temperature in the two types of Pickering emulsion systems, the yield in the W/O Pickering emulsions was always lower than that in the O/W Pickering emulsion system. It was observed (Fig. 6(b)) that, under Taylor flow along the microchannel, the length of the liquid slug (0.34 mm) formed in the O/W Pickering emulsions was shorter than that (0.43 mm) in the W/O Pickering emulsion system. That was attributed to the difference of the continuous phase viscosity in the two types of Pickering emulsion systems [36]. While the diffusion distance of O<sub>2</sub> in the continuous phase became shorter, it further strengthened the oxidation of benzyl alcohol and increased the yield of benzaldehyde in the O/W Pickering emulsion system. This demonstrated that the theoretical analysis results were largely consistent with the experimental observation in terms of benzaldehyde yield. It was clearly indicative that the oxidation reaction of benzyl alcohol in the O/W Pickering emulsion system was superior to that in the W/O Pickering emulsion system. Therefore, the O/W Pickering emulsion system was employed in the subsequent experiments as detailed below.

### 3.2. Effects of operational conditions on reaction performance

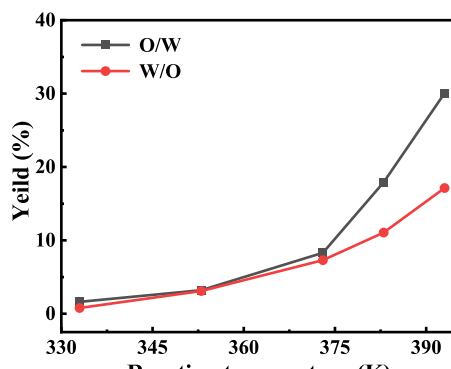
#### 3.2.1. Effects of reaction temperature

As expected, the conversion of benzyl alcohol increased with the increasing of reaction temperature (Fig. 7(a)) at all three CB levels of 3 wt%, 4 wt% and 5 wt%. That was mainly caused by the cleavage of alcohol OH bonds and the formation of alkoxy intermediates catalyzed by Pd promoted by the increased reaction temperature, thus intensifying the reaction process [47]. At a given temperature, the increased amount of catalyst (i.e., CB) resulted in a higher conversion, which was largely attributed to the increased numbers of active catalytic sites provided by the increased amount of solid catalyst particles.

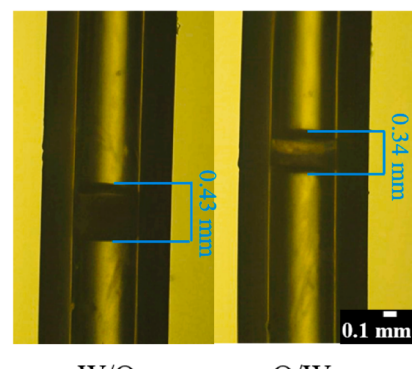
Fig. 7(b) shows the variation of benzaldehyde selectivity as a function of reaction temperature. At temperatures below 375 K, the selectivity remained remarkably high (approximately 100%) at all three CB levels. Above that critical temperature level, the benzaldehyde selectivity started to decline with the increasing of reaction temperature, though differed with different CB. Nevertheless, the overall selectivity was still high, greater than 99.6%, except for a single relatively low selectivity of 92.8% under the reaction conditions of 413 K and CB = 3.0 wt%. This was likely caused by the small amount of catalyst added which gave the lowest stability of the Pickering emulsion system among the three reaction systems.

It was observed that, when the reaction temperature reached 413 K, the droplet of emulsion turned into coalescence, which consequently led to decrease in the interfacial area of the specific phase while increase in the mass transfer distance. As a result, it limited the mass transfer process for the benzaldehyde produced on the interface of solid catalytic particles to be effectively extracted into the oil phase in time, causing its excessive oxidation and, in turn, the decrease in product benzaldehyde selectivity. It is suggested that the remarkably high selectivity observed in the oxidation of benzyl alcohol can be mainly attributed to the large interface area and short mass transfer distance exhibited in the Pickering emulsion system [48].

To understand the above-discussed demulsification phenomenon of the Pickering emulsion at high temperatures, the morphology of the Pickering emulsion droplets was characterized before and after the reaction under different conditions. As can be seen in Fig. 8, the diameter of the Pickering emulsion droplets after the reaction was generally larger than that before the reaction under all conditions applied. Particularly, it appeared to be more significant at the higher temperature of 413 K with a lower CB (3.0 wt%); the morphology of the droplets after the reaction changed significantly showing a violent flocculation (Fig. 8(b)). This further confirmed the above analysis that the decline of



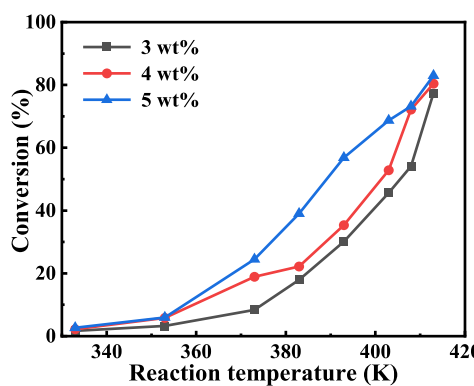
(a)



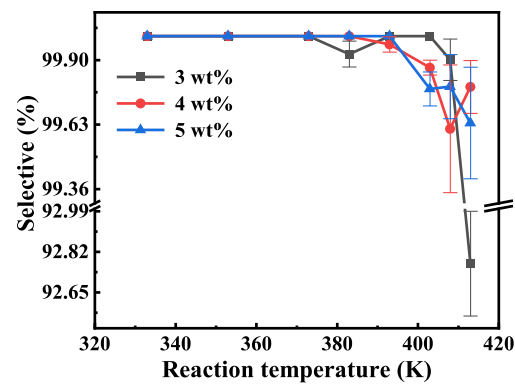
W/O                    O/W

(b)

**Fig. 6.** (a) Yield of benzaldehyde at varying temperature in O/W and W/O Pickering emulsions. (b) Comparison of liquid slug lengths in different Pickering emulsions in microchannels.  $V_{BNOH}/V_{Water} = 1$ ,  $O_2/BNOH$  (mol/mol) = 0.68, CB = 3.0 wt%, emulsion flow rate = 10  $\mu\text{L}/\text{min}$ , reaction tube length = 5.0 m.



(a)



(b)

**Fig. 7.** Effects of reaction temperature on (a) conversion of benzyl alcohol, and (b) product selectivity for the oxidation of benzyl alcohol at three CB levels (3.0 wt%, 4.0 wt% and 5.0 wt%).  $V_{BNOH}/V_{Water} = 1$ ,  $O_2/BNOH$  (mol/mol) = 0.68, emulsion flow rate = 10  $\mu\text{L}/\text{min}$ , reaction tube length = 5.0 m, residence time = 508 s.

benzaldehyde selectivity was largely attributed to the demulsification and aggregation of the Pickering emulsion.

### 3.2.2. Effects of the amount of catalytic solid particles

As discussed above the amount of catalytic solid particles affected the Pickering emulsion and, in turn, the reaction performance. This was further examined in terms of benzaldehyde yield under wider conditions, at four CB levels (2.0–5.0 wt%) and four temperatures (383–408 K). The results are shown in Fig. 9. Overall, the product yield increased in approximately a linear way with the increase in CB at all four temperature levels. As also expected, a higher temperature produced a higher yield.

In this reaction process, the solid catalytic nanoparticles of Pd/SiO<sub>2</sub> played dual functions, namely catalyst and emulsifier, and accordingly had two main effects on the oxidation reaction. On the one hand, the number of catalytic active sites in the system increased significantly with the increase of CB, which accelerated the oxidation rate of benzyl alcohol under the other identical conditions. On the other hand, the increase of CB reduced the diameter of emulsion droplets, where increased both the interface area of the oil–water two phases and the mass transfer rate of substances across the interface. In addition, an increase in the number of catalytic particles allowed more Pd/SiO<sub>2</sub> particles to enter the continuous phase, which further improved the stability of Pickering emulsion and reduced the coalescence of emulsion droplets in the multiphase reaction process.

It should be noted that when the value of CB was below 2.0 wt%, the

Pickering emulsion tended to undergo demulsification along the microchannel, resulting in a decrease in both the conversion and the selectivity. As it was above 5.5 wt%, nevertheless, a large number of catalytic solid particles entered into the continuous phase, which could be approximated as a suspension composed of solid particles and a continuous phase. Also, at high temperatures and low flow rates, the catalytic solid particles had more chances to adhere to the microchannel wall because the continuous phase of Pickering emulsion was in direct contact with the channel wall. Based on the above analysis, the CB range of 2.0 wt% to 5.5 wt% was considered to be appropriate for a stable operation in the given temperature range.

### 3.2.3. Effects of the volume of dispersed phase

The volume of the dispersed phase in emulsions can affect on both mass and heat transfer and, in turn, the reaction process. This effect was characterized in terms of benzaldehyde yield as a function of the volume ratio of oil to water ( $V_{BNOH}/V_{Water}$ ), by varying the volume of benzyl alcohol (i.e., dispersed phase), while the volume of aqueous phase and the amount of catalytic solid particles remained unchanged. Fig. 10 illustrates the experimental results at different temperatures and varied CB.

With the increase of  $V_{BNOH}/V_{Water}$  the yield of benzaldehyde decreased (Fig. 10(a)), which might be attributed to two main factors. On the one hand, with the increase of  $V_{BNOH}/V_{Water}$ , the average diameter of the emulsion droplets increased (Fig. 4), resulting in a decrease in the specific interface area between oil and water. It further led to an

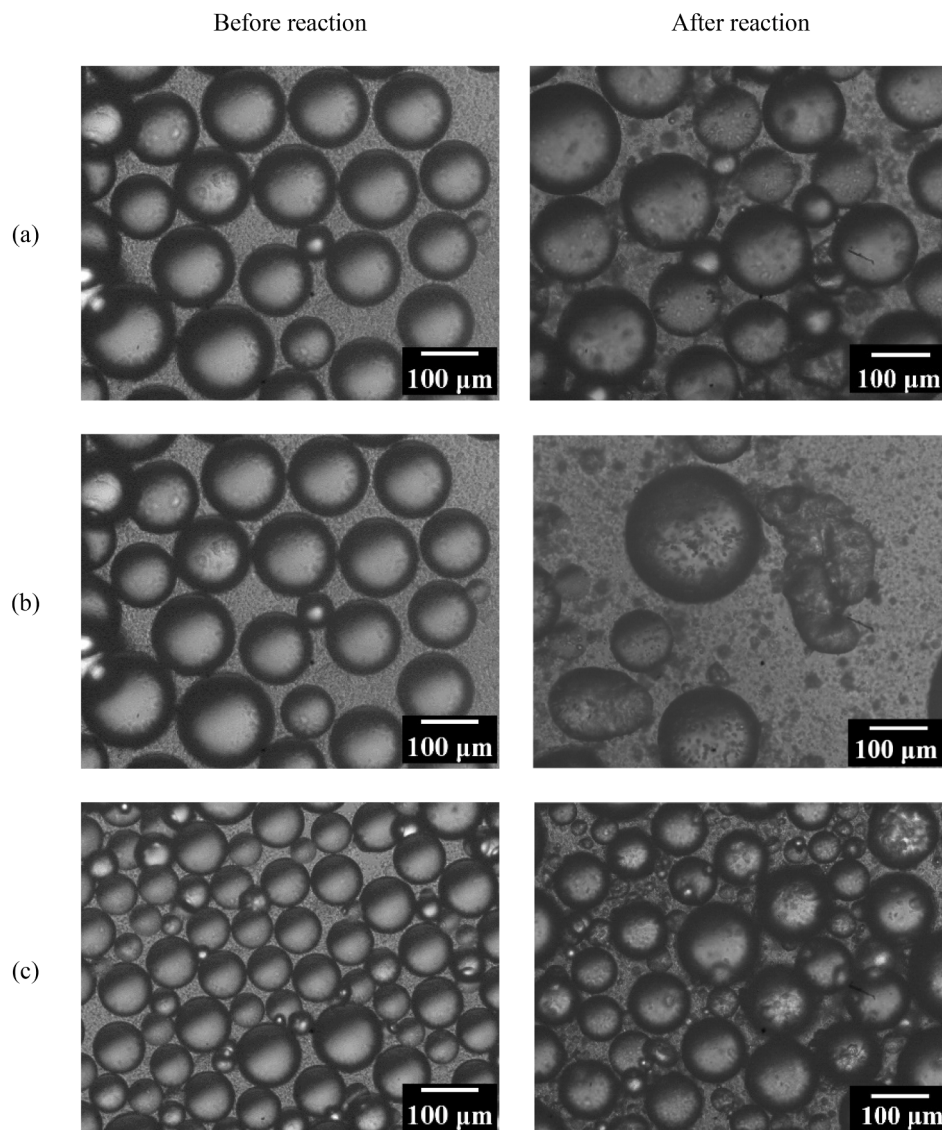


**Fig. 8.** Morphology changes of emulsion droplets before and after reaction under different conditions. (a)  $CB = 3.0$  wt%, 403 K, (b)  $CB = 3.0$  wt%, 413 K, (c)  $CB = 4.0$  wt%, 413 K.

increase in the mass transfer distance of reactants, whilst a decrease in the diffusion rate of reactants on the interface of two phases. On the other hand, the relative number of catalytic active sites in the system decreased with the increase of  $V_{BNOH}/V_{Water}$ , inhibiting the conversion of benzyl alcohol to benzaldehyde.

In order to compare the effects of the dispersed phase volume on the yield of benzaldehyde with the amount of catalytic solid particles, experiments were carried out to measure the product yield as a function of either the dispersed phase volume or the catalyst amount, individually, under comparable conditions.  $CB$  (The mass ratio of catalyst to benzyl alcohol) was used as abscissa to quantitatively compare the yield changes under two operating conditions. The experimental results depicted in Fig. 10(b). It was observed that the effects of these two parameters were largely equivalent on benzaldehyde yield. The results suggested that both decreasing the dispersed phase volume and increasing the amount of catalytic solid particles can result in higher product yields under the reaction conditions examined.

#### 3.2.4. Effects of varying reactor microchannel length

The variation in the reactor microchannel length can affect the residence time of the fluid within the reactor and the pressure drop

along the microchannel, thus altering the reaction time, mass transfer and, ultimately the reaction performance. These effects were characterized by varying the reactor microchannel (or tube) length in the range of 0.5–8.0 m under identical operating conditions. The experiment results are plotted in Fig. 11. The reaction conversion, selectivity and total (gas–liquid–solid) volumetric flow rate as a function of tube length at three temperature levels of 383 K, 393 K and 403 K are investigated.

As displayed in Fig. 11(a), the conversion of benzyl alcohol increased approximately linearly with the increase of the reactor tube length, though tending to level off with further longer tube. The overall profile trend appeared at all three temperature levels, where a higher temperature resulted in a faster reaction rate as expected. It was clearly found that the selectivity of benzaldehyde was mostly greater than 99.7%, although a very slight drop was seen in the longer lengths (Fig. 11(b)). Under the experimental conditions, the flow pattern of the gas–liquid two phases in the microchannel was generally maintained as slug flow, the most stable flow pattern in the gas–liquid multiphase microfluidics.

The effects on benzaldehyde yield by increasing the tube length could be explained in threefold. Firstly, with the increase of tube length, the residence time of reactants in the microchannel increased, providing a longer reaction time for the benzyl alcohol to be converted into

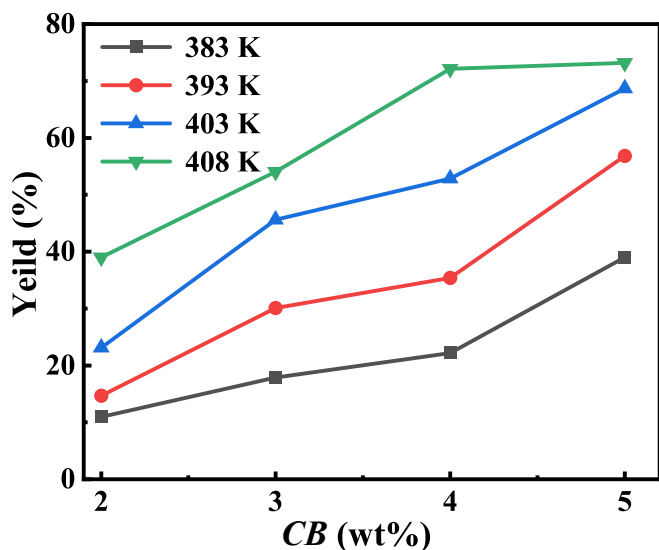


**Fig. 9.** Effects of the amount of catalytic solid particles on benzaldehyde yield.  $V_{BNOH}/V_{Water} = 1$ ,  $O_2/BNOH$  (mol/mol) = 0.68, reaction tube length = 5.0 m, emulsion flow rate = 10  $\mu\text{L}/\text{min}$ .

benzaldehyde. As the tube length increased with longer residence time and further progress of reaction, secondly, more gas phase oxygen was consumed, leading to a decrease in the total volumetric flow rate of the multiphase flow, as shown in Fig. 11(c). Finally, the pressure drop along the reactor microchannel exhibited an increase trend with the increase of tube length as expected. That was advantageous for the diffusion of oxygen molecules into a continuous aqueous phase and had a positive impact on the yield of benzaldehyde. Under experimental operating conditions, in general, the three factors discussed above actively interacted together to promote the conversion of benzyl alcohol and increase the yield of benzaldehyde in the microchannel reactor.

### 3.2.5. Effects of total volumetric flow rate

With a given residence time and constant tube diameter, a longer tube is needed to achieve a higher total volumetric flow rate. However, varying total volumetric flow rate may have more complicated influence on hydrodynamics, mass transfer and ultimately the reaction. Therefore, this was more closely investigated. Fig. 12 depicts the profiles of product yield as a function of total flow rate at three temperature levels, and visual observation.

As seen in Fig. 12(a), at a given reaction temperature the product yield profile changed through two stages, a rapid increase followed by

leveling off at a relatively stable level. The critical turning point was around the total volumetric flow rate of 820  $\mu\text{L}/\text{min}$  in all three profiles. Also, a higher temperature resulted in a higher yield while all three profiles of product yield showed a similar trend.

As discussed, in order to keep a constant residence time, different lengths of tubes with a given inner diameter were used at different total volumetric flow rates. It was observed that when the total flow rate increased at a given gas-liquid flow ratio, the length of gas bubbles decreased noticeably, from 2.51 mm to 1.95 mm in responding to the total flow rate increase from 550  $\mu\text{L}/\text{min}$  to 1720  $\mu\text{L}/\text{min}$ , as observed in the middle of the reactor tube (Fig. 12(b)). This reduction in gas bubble size further led to an increase in the interfacial area between gas and emulsion phases, thus enhancing interfacial mass transfer performance. This was in line with the above investigation on the effect of tube length (Fig. 11(c)). Furthermore, this flow pattern change enhanced the internal circulation of liquid plug and mass transfer across gas-liquid interface with the increase of the total volume flow rate. Therefore, the conversion of benzyl alcohol and the yield of benzaldehyde increased with the increase of the total volume flow rate (<820  $\mu\text{L}/\text{min}$ ). When the volume flow rate was greater than 820  $\mu\text{L}/\text{min}$ , the yield of benzaldehyde was almost unchanged with the increase of the total volume flow rate. This indicated that the effect of the mass transfer resistance on the conversion of benzyl alcohol could be neglected at the higher total volume flow rates (greater than 820  $\mu\text{L}/\text{min}$ ), and the oxidation reaction of benzyl alcohol was controlled by the intrinsic kinetics in the range of the total volumetric flow rate.

### 3.2.6. Effects of the volumetric flow rate ratio of gas/liquid two phases

As demonstrated above, the variation of gas bubble size clearly affected the interfacial mass transfer area, and thus the reaction performance. This was further investigated by varying the volumetric flow rate ratio in a wider range of 81–117, by changing the gas volumetric flow rate in the range of 810–1170  $\mu\text{L}/\text{min}$  whilst keeping liquid volumetric flow rate at 10  $\mu\text{L}/\text{min}$  constant. Fig. 13 displays the profiles of product yield as a function of gas/liquid volumetric flow ratio at two temperature levels, and visual observation. The experimental results (Fig. 13(a)) showed that the yield of benzaldehyde increased initially with the increase of gas/liquid flow rate ratio, reached a maximum point at a flow rate ratio of 99, that was followed by a decline. This trend exhibited at both temperature levels, where a higher temperature resulted in a higher product yield as expected.

There were two main factors contributing to the increase of benzaldehyde yield. On the one hand, the total volumetric flow rate became larger with the increase of gas flow rate, which enhanced the internal circulation in the liquid plug. This further accelerated the regeneration

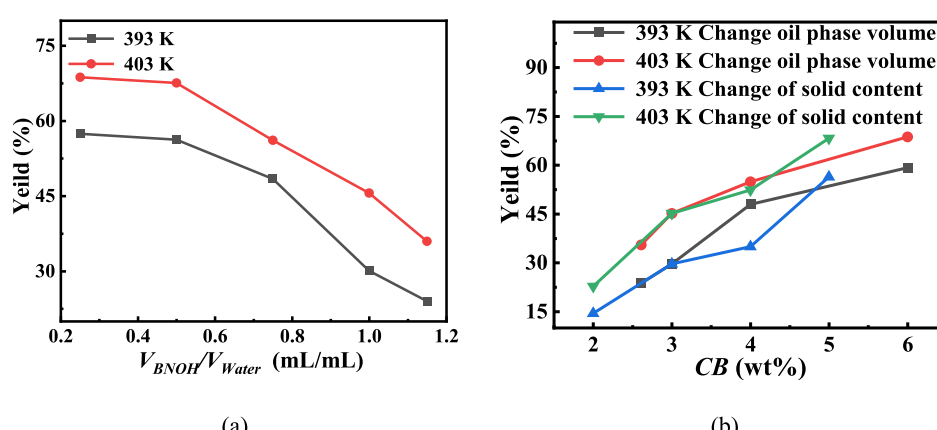


**Fig. 10.** (a) Effects of oil phase volume on the yield of benzaldehyde at 393 K and 403 K. (b) Comparison of effects of oil phase volume and catalyst addition on benzaldehyde yield. Catalyst amount = 0.06 g; Reaction tube length = 5.0 m; Emulsion flow rate = 10  $\mu\text{L}/\text{min}$ .

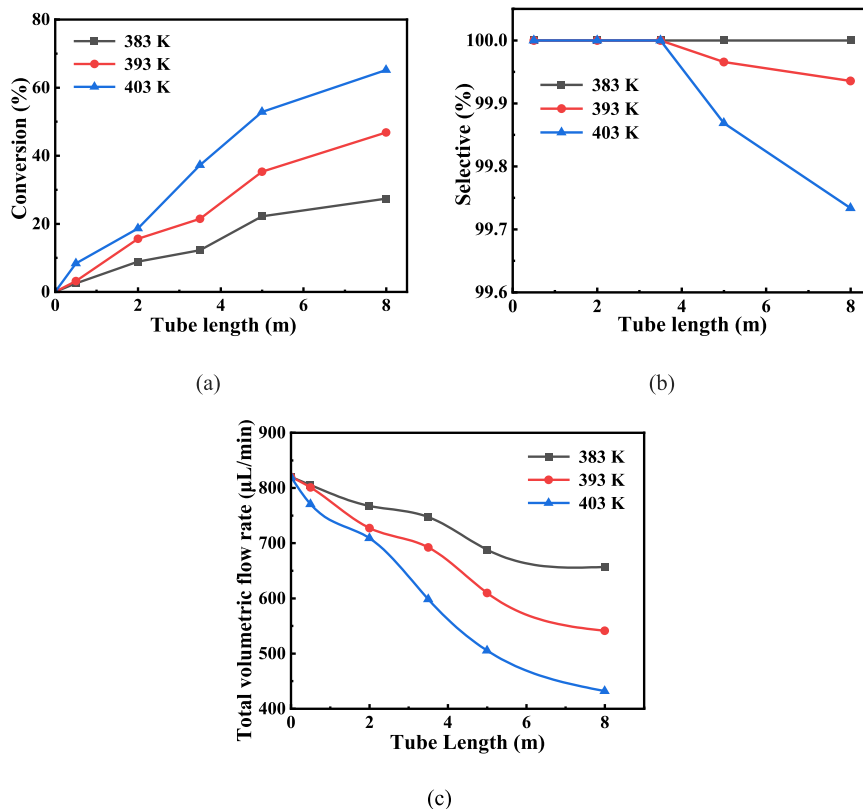


**Fig. 11.** Effects of tube length on (a) conversion of benzyl alcohol, (b) selectivity of benzaldehyde, and (c) total volumetric (gas–liquid–solid) flow rate.  $V_{BNOH}/V_{Water} = 1$ ,  $O_2/BNOH$  (mol/mol) = 0.68,  $CB$  = 4.0 wt%, emulsion flow rate = 10  $\mu\text{L}/\text{min}$ .

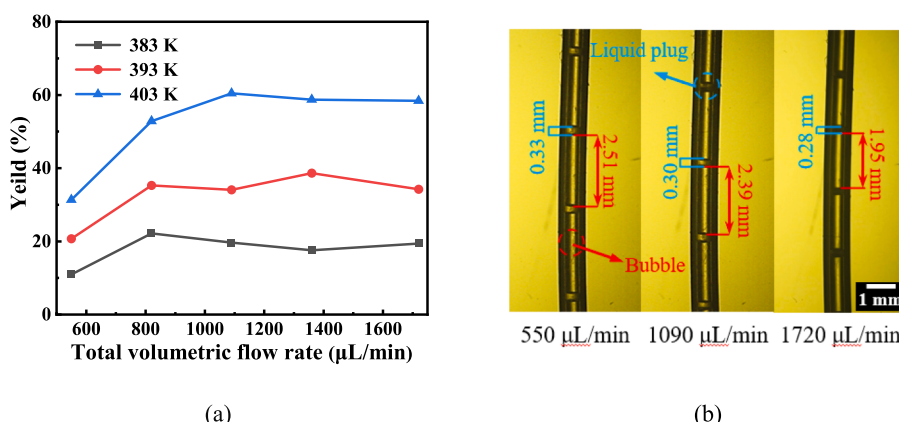
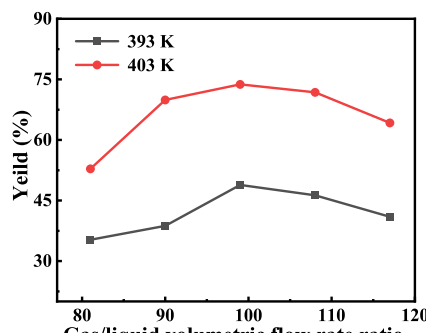


**Fig. 12.** (a) Effects of total volumetric flow rate on benzaldehyde yield at 383 K, 393 K and 403 K. (b) Micrographs showing different flow states at total flow rates of 550  $\mu\text{L}/\text{min}$ , 1090  $\mu\text{L}/\text{min}$  and 1720  $\mu\text{L}/\text{min}$ .  $V_{BNOH}/V_{Water} = 1$ ,  $O_2/BNOH$  (mol/mol) = 0.68,  $CB$  = 4 wt%.

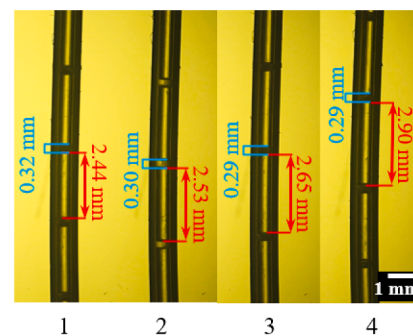
rate of the liquid film side of the gas–liquid interface, and led to enhanced mass transfer performance in the liquid phase. On the other hand, the gas bubble length increased with the increase in gas flow rate while the liquid plug length almost remained constant in the process (Fig. 13(b)), from 2.44 mm to 2.90 mm corresponding to gas flow rate increased from 900  $\mu\text{L}/\text{min}$  to 1170  $\mu\text{L}/\text{min}$ , as observed in the middle of the reactor tube. This provided a larger interface area between the gas and liquid phases, and thus a higher mass transfer rate of  $O_2$  to the liquid phase.

As the ratio of gas volumetric flow rate to liquid volumetric flow was higher than the critical value of 99, the yield of benzaldehyde started to decline slightly with the increase of the flow rate ratio (Fig. 13(a)). This

was mainly a result of the fixed reactor tube length of 5.0 m in the experiments. With the given tube length the residence time of reactants in the microchannel reduced with the increase in gas flow rate, thus total flow rate. It was observed that under these operating conditions, the effects of the reduction in residence time on the yield of benzaldehyde were significantly stronger than that of the enhancement of mass transfer process, therefore, the yield of benzaldehyde decreased. Under these experimental conditions, the optimal yield of benzaldehyde was found at the gas–liquid volumetric flow rate ratio of 99 for both temperature levels of 393 K and 403 K.



(a)



(b)

**Fig. 13.** (a) Effect of gas–liquid two-phase volumetric flow rate on the yield of benzaldehyde. (b) Micrographs showing changes of the flow state with different flow rate ratios at gas flow rates of (1) 900  $\mu\text{L}/\text{min}$ , (2) 990  $\mu\text{L}/\text{min}$ , (3) 1080  $\mu\text{L}/\text{min}$ , and (4) 1170  $\mu\text{L}/\text{min}$ .  $V_{\text{BNOH}}/V_{\text{Water}} = 1$ ,  $\text{CB} = 4.0 \text{ wt\%}$ , reaction tube length = 5.0 m.

### 3.2.7. Effects of the reactor tube inner diameter

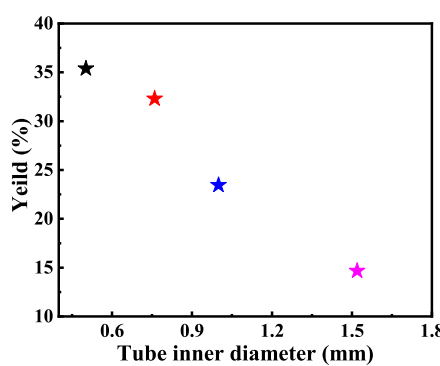
It is well known that the size of the reactor tube inner diameter has a great influence on the gas–liquid flow dynamics in the microchannel as the linear velocity of the fluid changes at a given volumetric flow rate, that further affect the mass transfer and ultimately the reaction outcomes. Fig. 14 depicted the influence of the reactor tube inner diameter on the yield of the benzaldehyde and the flow state within the microchannel operated at a constant volumetric flow rate. When the reactor tube inner diameter decreased from 1.59 mm to 0.5 mm, the yield of benzaldehyde increased approximately in linear from 14.67% to 35.39%. This was primarily due to the fact that the mixing process in the liquid phase and the mass transfer process between two phases were enhanced by decreasing the inner diameter of microchannel. Firstly, as the total volumetric flow rate and gas–liquid flow rate ratio were kept constant (e.g., 99  $\mu\text{L}/\text{min}$ ), the overall apparent linear velocity increased with the decrease of the inner diameter. Subsequently, the internal circulation and mixing in the liquid plug were enhanced, as discussed above, which accelerated the regeneration rate of the liquid film side at the gas–liquid phase interface and enhanced the mass transfer in the liquid phase. Secondly, when the tube inner diameter decreased, the formation frequencies of bubbles and liquid plugs increased, on the contrary, the lengths of bubbles and liquid plugs decreased accordingly, as evidenced in the experiments with the inner diameters of 0.5 and 1.59 mm displayed in Fig. 14(b). In that case, the specific phase interface area between the gas and liquid phases and the mass transfer rate of  $\text{O}_2$  to the liquid phase increased, respectively. Finally, in order to keep the total volume of the microchannel constant, the length of the tube must be extended due to the reduction of its inner diameter. The pressure drop

in the extended tube increased, and subsequently the pressure of dispersed bubbles in the microchannel increased, which further promoted the mass transfer of  $\text{O}_2$  into the liquid phase. Based on the combination of these above factors, the yield of benzaldehyde showed an increasing trend with the decrease of tube inner diameter.

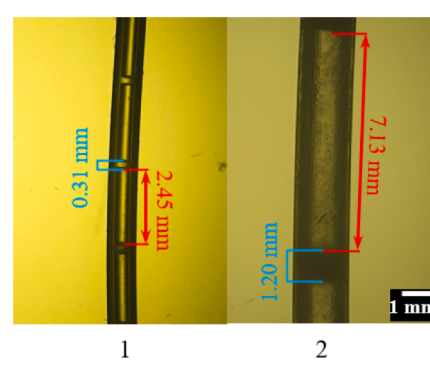
### 3.3. Interfacial catalytic mechanism of Pickering emulsion in microchannels

This is a complex system involving Pickering emulsion enhanced multiphase (gas–liquid–solid) catalytic reaction under Taylor flow along microchannel, influenced by a number of factors as demonstrated above. In order to further understand the interaction between various factors on the catalytic oxidation of benzyl alcohol, the interfacial catalytic mechanism in Pickering emulsion was established in this study from the perspective of mass transfer between multiple phases in microchannels. Based on previous research on mass transfer process in related systems, a unit-cell model [49] was usually constructed including gas bubbles, liquid slugs & Pickering emulsion, and liquid films on channel wall. The model is schematically shown in Fig. 15.

On the one hand, there was the thin film between the bubble and the channel wall in the slug flow pattern, which provided a large phase interface area and intensified the mass transfer of  $\text{O}_2$  from gas phase to the continuous phase. On the other hand, there was an internal circulation in the continuous liquid phase of the multiphase flow system, which was presented as a centrally symmetrical distribution as shown in Supplementary (Video 1) that was consistent with the unit-cell model (Fig. 15). The internal circulation in the continuous phase accelerated



(a)



(b)

**Fig. 14.** (a) Effects of reactor tube inner diameter on the yield of benzaldehyde. (b) Micrographs of different tube inner diameters showing different flow states with an inner diameter of (1) 0.5 mm, and (2) 1.59 mm.  $V_{\text{BNOH}}/V_{\text{Water}} = 1$ ,  $\text{O}_2/\text{BNOH}$  (mol/mol) = 0.68,  $\text{CB} = 4.0 \text{ wt\%}$ ,  $T = 393 \text{ K}$ .

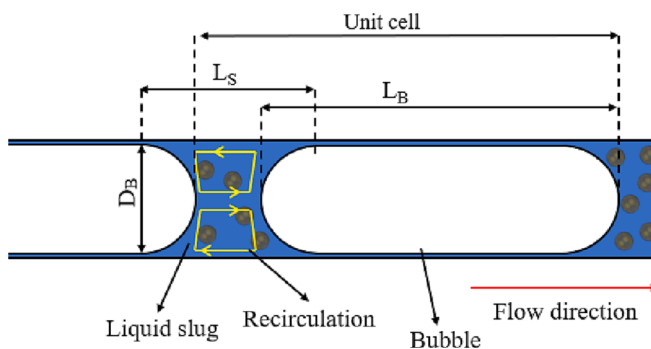


**Fig. 15.** Unit-cell model of Taylor flow with Pickering emulsion along microchannel.

the regeneration rate of the liquid film side at the gas–liquid phase interface and enhanced the mixture in the liquid phase body.

In order to understand the mass transfer process and the control step of the catalytic oxidation of benzyl alcohol within the multiphase flow system, a schematic diagram of the mass transfer process for the Pickering emulsion-O<sub>2</sub> system in a microchannel is shown in Fig. 16. Since the multiphase flow system contained gas phase, oil phase, water phase, and solid phase, the mass transfer process of the system was very complicated, involving multiple mass transfer paths. On the one hand, the catalytic oxidation reaction of benzyl alcohol mainly took place in the continuous aqueous phase. The mass transfer paths involved in this process included the oxygen molecules diffusing from the bubble into the continuous phase and the benzyl alcohol diffusing from the dispersed droplets of oil phase into the continuous aqueous phase. In the continuous phase, the benzyl alcohol reacted with oxygen catalyzed by Pd/SiO<sub>2</sub> catalyst particles, which were dispersed in the continuous phase because they were in excess during the preparation of the Pickering emulsion. Subsequently, the product benzaldehyde was extracted into the dispersed droplets of oil phase.

On the other hand, the catalytic oxidation reaction of benzyl alcohol also occurred on the oil phase side of the oil–water interface. The mass transfer in this process mainly underwent through the following paths. (i) Oxygen molecules diffused from the bubble into the continuous phase and then entered the oil phase side of the oil–water interface. (ii) On the oil–water interface, the oxygen reacted with the benzyl alcohol from the dispersed droplet catalyzed by Pd/SiO<sub>2</sub> catalyst particles, which were dispersed on the oil–water interface to stabilize the Pickering emulsion. (iii) Water produced from the reaction was extracted into the continuous aqueous phase, while the benzaldehyde generated in the process remained in the dispersed droplets of oil phase. Since the catalytic oxidation of benzyl alcohol was a fast reaction, the reaction process was mainly controlled by the mass transfer process, as demonstrated by the

above experiments. Based on the above analysis of the mass transfer paths, the mass transfer process involved two interfaces, i.e., the gas–liquid interface and the oil–water interface. Therefore, increasing the interface area of either or both of the two interfaces was beneficial for the intensification of the mass transfer process.

Then, the approaches to increasing the interface area were further analyzed, as follows. Since the oxygen was more excessive than the reactant benzyl alcohol in the reaction process, the bubble shape always remained ellipsoidal, namely keeping a slug flow in the flow system. In the study, the head and tail of the bubble were treated as hemispheres with the diameter of D<sub>B</sub>, and the body of the bubble was considered as a cylinder. Therefore, the surface area of the single bubble (S) can be expressed by:

$$S = \pi D_B L_B \quad (12)$$

where L<sub>B</sub> is the bubble length as shown in the above unit-cell model (Fig. 15). It was assumed that D<sub>B</sub> did not change when the bubble flowed along the channel. Thus, the volume of single bubble (V) was calculated from the following equation:

$$V = \frac{\pi D^2 (L_S - D_B + L_B)}{4} \quad (13)$$

where D is the microchannel diameter and L<sub>S</sub> is the liquid plug length. Because the film between the bubble and the channel wall in the slug flow pattern was very thin, the value of D<sub>B</sub> can be approximated to that of D. Finally, Eq. (13) can be rewritten as:

$$V = \frac{\pi D_B^2 (L_S - D_B + L_B)}{4} \quad (14)$$

Combined with Eqs. (12) and (14), the following equation can be obtained:

$$\frac{S}{V} = \frac{4L_B}{D_B(L_S - D_B + L_B)} = \frac{1}{D_B} \frac{4}{\left(1 + \frac{L_S - D_B}{L_B}\right)} \quad (15)$$

It can be seen from the above Eq. (15) that the larger  $\frac{S}{V}$  value is conducive to the mass transfer between gas and liquid phases, which is mainly controlled by both the lengths of the bubble and the liquid plug. The changes associated with the lengths of the bubble and liquid plug were influenced by various factors. Firstly, as the catalytic oxidation reaction of benzyl alcohol continuously progressed, the oxygen was consumed and the volume of bubble decreased. This resulted in a decrease in the length of the bubble, which in turn led to a decrease in the  $\frac{S}{V}$ . Secondly, the lengths of the bubble and liquid plug were influenced by the volumetric flow rate of gas phase. When the volumetric flow rate of liquid phase was fixed, the length of the bubble in the microchannel increased with the increasing of the volumetric flow rate of gas phase. In contrast, the length of the liquid plug decreased with the

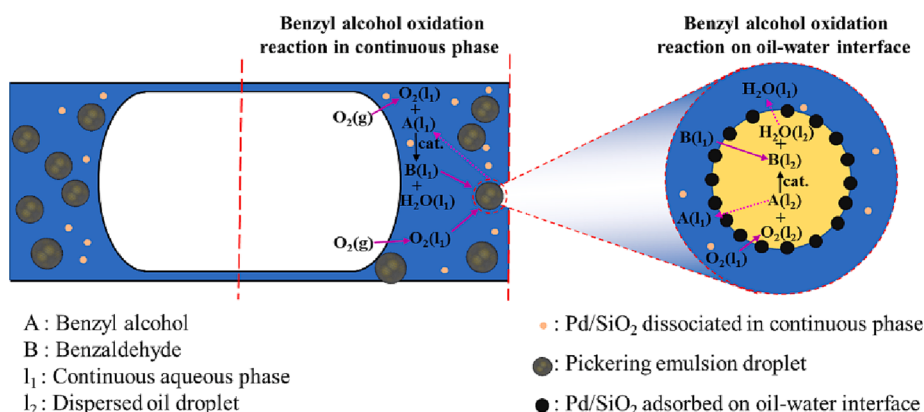


**Fig. 16.** Schematic diagram of mass transfer process for the Pickering emulsion-O<sub>2</sub> system in a microchannel.

increasing of the volumetric flow rate of gas phase. Because the length of the liquid film between the bubble and the channel wall increased with the increasing of the length of bubble, if the volumetric flow rate of gas phase continues to increase, the liquid plug tended to disappear and the flow regime in the microchannel can become an annular flow, in line with our previous observation [50]. Thus, the value  $\frac{S}{V}$  increased with the increasing of the volumetric flow rate of gas phase. Finally, the lengths of the bubble and liquid plug were also affected by the volumetric flow rate of liquid phase. When the volumetric flow rate of gas phase kept constant and the volumetric flow rate of liquid phase increased, the experimental results were adverse to those associated with the increasing of the volumetric flow rate of gas phase.

By varying operating variables, the interface area between oil and water phases can be regulated. The amount of catalyst particles played an important role in determining the oil–water interface area. It was firstly assumed that the dimension of all oil droplets in the Pickering emulsion was uniform and owned the same diameter. Thus, the oil–water interface area ( $S_{OW}$ ) in the Pickering emulsion can be expressed by:

$$S_{OW} = \frac{6V_{Oil}}{D_D} \quad (16)$$

where  $V_{Oil}$  is the volume of benzyl alcohol and  $D_D$  is the droplet diameter of the Pickering emulsion.

By experiments to measure the droplet diameter with different amount of catalyst particles added, the oil–water interface area was obtained by Eq. (16). The results are shown in Fig. 17. It could be seen from the figure that when the volume of benzyl alcohol and water was fixed at 2.0 mL, the droplet diameter significantly decreased and the oil–water interface area sharply increased with an increase in the amount of catalyst particles. When the amount of catalyst particles increased from 0.04 g to 0.10 g, the droplet diameter decreased from 206.93  $\mu\text{m}$  to 54.19  $\mu\text{m}$ , and the oil–water interface area simultaneously increased from 579.91  $\text{cm}^2$  to 2214.43  $\text{cm}^2$ , respectively, which was equivalent to a four-fold increase in the oil–water interface area. In addition, a larger droplet diameter due to the lower amount of catalyst particles resulted in a poor stability of the Pickering emulsion, as demonstrated in the previous section. Once the demulsification and coalescence of droplets in the Pickering emulsion occurred, the interfacial area between oil and water phases decreased sharply.

Another important operating variable influencing the oil–water interface area was the volume of the dispersed oil phase. The experimental results (Fig. 18) indicated that by fixing the amount of catalytic solid particles and the volume of the water phase, the droplet diameter significantly increased with the increasing of the volume of the dispersed oil phase. This was mainly due to the fact that there were

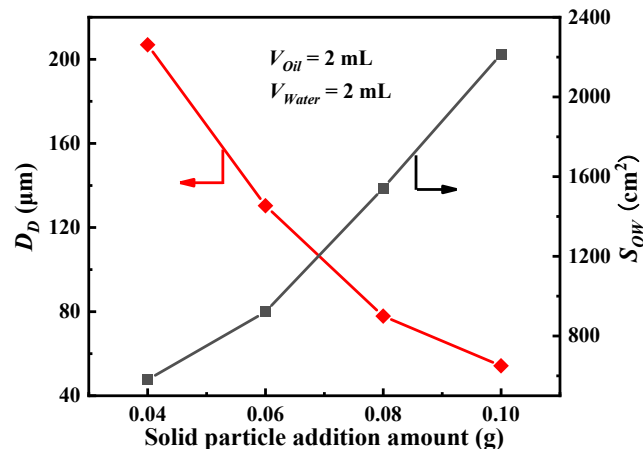


Fig. 17. Effects of the amount of catalyst particles on droplet diameter and oil–water interface area.

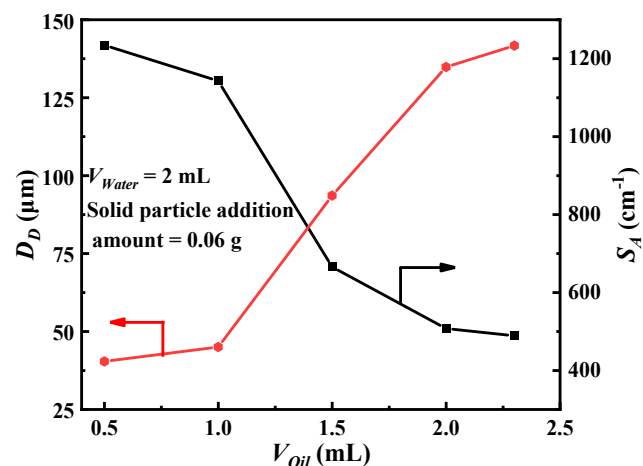


Fig. 18. Effects of dispersed oil phase volume on droplet diameter and specific interface area.

insufficient catalytic solid particles to cover the oil–water interface with increasing volume of the dispersed oil phase. Since the volume of the dispersed oil phase was not kept constant, it was difficult to only determine the oil–water interface area as an absolute quantity. Thus, the new parameter, namely, specific interface area ( $S_A$ ) was introduced to analyze the effects of the dispersed oil phase volume on the oil–water interface area, which was defined as:

$$S_A = \frac{S_{OW}}{V_{Oil}} \quad (17)$$

Combined with Eqs. (16) and (17), the final  $S_A$  was expressed as:

$$S_A = \frac{6}{D_D} \quad (18)$$

As shown in Fig. 18, the value of  $S_A$  decreased when the volume of the dispersed phase increased, as expressed in Eq. (18), being inversely proportional to  $D_D$ . Based on the above analysis, it can be concluded that the effects of reducing the dispersed phase volume on the oil–water interface area was equivalent to the effect of increasing the amount of catalytic solid particles on the specific interface area.

#### 4. Conclusion

The fouling and clogging of microchannels caused by solid particles hinder the application of microchannel reactors for multiphase catalytic reactions involving solid particles. In this study, the Pickering emulsion assisted gas–liquid–solid multiphase catalytic oxidation of benzyl alcohol in microchannel reactors under Taylor flow was systematically investigated, both experimentally and theoretically. Effects of a wide range of operational parameters on flow hydrodynamics, mass transfer and reaction performance were investigated, including reaction temperature, amount of catalytic solid particles, oil–water phase volume ratio, reactor tube length, total flow rate, gas–liquid phase volumetric flow rate ratio and microchannel reactor tube diameter. Furthermore, theoretical analysis was conducted to investigate the interaction of various factors on the catalytic oxidation of benzyl alcohol. The interfacial catalytic process mechanism was established from the perspective of mass transfer between multiple phases.

- (1) Compared to W/O Pickering emulsions, O/W Pickering emulsions showed better performance for the catalytic oxidation of benzyl alcohol in terms of product yield of benzaldehyde.
- (2) Higher catalyst to benzyl alcohol mass ratios (CB) provided higher stability of Pickering emulsion in the reaction process and higher product selectivity by eliminating droplet coalescences.

- (3) When CB was below 2.0 wt%, the Pickering emulsion tended to undergo demulsification during the continuous flow process, whilst higher CB (above 5.5 wt%) resulted in the catalytic solid particles to adhere to the microchannel wall, particularly at high temperatures and low flow rates. The optimal CB range was found to be 2.0–5.5 wt% under the operation conditions.
- (4) The yield of product benzaldehyde increased with the increase of total volumetric flow rate before levelling off at 820  $\mu\text{L}/\text{min}$ , indicating that the effect of mass transfer resistance on the conversion of benzyl alcohol was neglectable at the higher total volumetric flow rates ( $>820 \mu\text{L}/\text{min}$ ), where the reaction process was controlled by the intrinsic kinetics.
- (5) A mass transfer model was proposed mapping the mass transfer pathways in the Pickering emulsion assisted catalytic oxidation of benzyl alcohol in a Taylor flow microchannel reactor in order to gain insights into the mechanism of the multiphase transport-reaction system, involving mass transfer across both gas–liquid and oil–water interfaces. Methods for regulating the interface areas of gas–liquid and oil–water phases were further developed.

### Declaration of Competing Interest

The authors declare that they have no known competing financial interests or personal relationships that could have appeared to influence the work reported in this paper.

### Data availability

Data will be made available on request.

### Acknowledgements

We gratefully acknowledge the financial supports from National Natural Science Foundation of China (Nos. 21978250, 22208278) and Natural Science Foundation of Shandong Province (ZR2020KB013, ZR2020QE211, 2019KJC012).

### Appendix A. Supplementary data

Supplementary data to this article can be found online at <https://doi.org/10.1016/j.cej.2023.143258>.

### References

- [1] W. Ehrfeld, V. Hessel, H. Löwe, *Microreactors: New Technology for Modern Chemistry*, WILEY-VCH, Weinheim, 2000, pp. 33–36.
- [2] F. Fanelli, G. Parisi, L. Degennaro, R. Luisi, Contribution of microreactor technology and flow chemistry to the development of green and sustainable synthesis, *Beilstein J. Org. Chem.* 13 (2017) 520–542.
- [3] D. Dallinger, B. Gutmann, C.O. Kappe, The concept of chemical generators: On-site on-demand production of hazardous reagents in continuous flow, *Acc. Chem. Res.* 53 (2020) 1330–1341.
- [4] Y.C. Zhao, G.W. Chen, C.B. Ye, Q. Yuan, Gas-liquid two-phase flow in microchannel at elevated pressure, *Chem. Eng. Sci.* 87 (2013) 122–132.
- [5] J. Tan, Y.C. Lu, J.H. Xu, G.S. Luo, Mass transfer performance of gas-liquid segmented flow in microchannels, *Chem. Eng. J.* 181 (2012) 229–235.
- [6] J. Yue, G. Chen, Q. Yuan, L. Luo, Y. Gonthier, Hydrodynamics and mass transfer characteristics in gas-liquid flow through a rectangular microchannel, *Chem. Eng. Sci.* 62 (7) (2007) 2096–2108.
- [7] Y. Song, M.J. Shang, J.G. Li, Y.H. Su, Continuous and controllable synthesis of MnO<sub>2</sub>/PPy composites with core-shell structures for supercapacitors, *Chem. Eng. J.* 405 (2021), 127059.
- [8] M. Al-Rawashdeh, L.J.M. Fluitmans, T.A. Nijhuis, E.V. Rebrov, V. Hessel, J. C. Schouten, Design criteria for a barrier-based gas-liquid flow distributor for parallel microchannels, *Chem. Eng. J.* 181 (2012) 549–556.
- [9] Y.P. Dong, C.Y. Zhu, Y.G. Ma, T.T. Fu, Distribution of liquid-liquid two-phase flow and droplet dynamics in asymmetric parallel microchannels, *Chem. Eng. J.* 441 (2022), 136027.
- [10] F. Ebrahimi, T. Virkki-Hatakka, I. Turunen, Safety analysis of intensified processes, *Chem. Eng. Process.* 52 (2012) 28–33.
- [11] F. Ebrahimi, E. Kolehmainen, I. Turunen, Safety advantages of on-site microprocesses, *Org. Process Res. Dev.* 13 (5) (2009) 965–969.
- [12] L. Sicignano, G. Tomaiuolo, A. Perazzoa, S.P. Nolan, P.L. Maffettone, S. Guido, The effect of shear flow on microreactor clogging, *Chem. Eng. J.* 341 (2018) 639–647.
- [13] J. Yue, Multiphase flow processing in microreactors combined with heterogeneous catalysis for efficient and sustainable chemical synthesis, *Catal. Today* 308 (2018) 3–19.
- [14] A. Tanimu, S. Jaenicke, K. Alhooshani, Heterogeneous catalysis in continuous flow microreactors: A review of methods and applications, *Chem. Eng. J.* 327 (2017) 792–821.
- [15] K.S. Elvira, X.C. i Solvas, R.C.R. Wootton, A.J. deMello, The past, present and potential for microfluidic reactor technology in chemical synthesis, *Nat. Chem.* 5 (11) (2013) 905–915.
- [16] G. Chen, S. Li, Q. Yuan, Pd-Zn/Cu-Zn-Al catalysts prepared for methanol oxidation reforming in microchannel reactors, *Catal. Today* 120 (1) (2007) 63–70.
- [17] L. He, Y.L. Fan, L.A. Luo, J. Bellettre, J. Yue, Preparation of Pt/ $\gamma$ -Al<sub>2</sub>O<sub>3</sub> catalyst coating in microreactors for catalytic methane combustion, *Chem. Eng. J.* 380 (2019), 122424.
- [18] J. Zong, J. Yue, Continuous solid particle flow in microreactors for efficient chemical conversion, *Ind. Eng. Chem. Res.* 61 (19) (2022) 6269–6291.
- [19] A.K. Liedtke, F. Bornette, R. Philippe, C. de Bellefon, Gas-liquid-solid “slurry Taylor” flow: Experimental evaluation through the catalytic hydrogenation of 3-methyl-1-pentyn-3-ol, *Chem. Eng. J.* 227 (2013) 174–181.
- [20] N. Al-Rifai, F. Galvanin, M. Morad, E.H. Cao, S. Cattaneo, M. Sankar, V. Dua, G. Hutchings, A. Gavriliidis, Hydrodynamic effects on three phase micro-packed bed reactor performance-gold-palladium catalysed benzyl alcohol oxidation, *Chem. Eng. Sci.* 149 (2016) 129–142.
- [21] N. Márquez, P. Castaño, J.A. Moulijn, M. Makkee, M.T. Kreutzer, Transient behavior and stability in miniaturized multiphase packed bed reactors, *Ind. Eng. Chem. Res.* 49 (3) (2010) 1033–1040.
- [22] C. Zhang, X. Duan, J. Yin, F. Lou, J. Zhang, Copper/TEMPO-catalyzed continuous aerobic alcohol oxidation in a micro-packed bed reactor, *React. Chem. Eng.* 7 (6) (2022) 1289–1296.
- [23] E. Cao, M. Sankar, S. Firth, K.F. Lam, D. Bethell, D.K. Knight, G.J. Hutchings, P. F. McMillan, A. Gavriliidis, Reaction and Raman spectroscopic studies of alcohol oxidation on gold-palladium catalysts in microstructured reactors, *Chem. Eng. J.* 167 (2–3) (2011) 734–743.
- [24] P. Stavarek, Z. Vajglova, J. Kristal, V. Jiricny, J. Kolena, Self-sustained oscillations of temperature and conversion in a packed bed microreactor during 2-methylpropene (isobutene) hydrogenation, *Catal. Today* 256 (2015) 250–260.
- [25] A. Ufer, D. Sudhoff, A. Mescher, D.W. Agar, Suspension catalysis in a liquid-liquid capillary microreactor, *Chem. Eng. J.* 167 (2–3) (2011) 468–474.
- [26] A.-K. Liedtke, F. Scheiff, F. Bornette, R. Philippe, D.W. Agar, C. de Bellefon, Liquid-solid mass transfer for microchannel suspension catalysis in gas-liquid and liquid-liquid segmented flow, *Ind. Eng. Chem. Res.* 54 (17) (2015) 4699–4708.
- [27] F. Scheiff, D.W. Agar, Solid particle handling in microreaction technology: Practical challenges and application of microfluid segments for particle-based processes, in: J. Michael Köhler, B.P. Cahill (Eds.), *Micro-segmented flow applications in chemistry and biology*, Springer, Berlin Heidelberg, 2013, pp. 103–148.
- [28] M. Schoenitz, L. Grundemann, W. Augustin, S. Scholl, Fouling in microstructured devices: A review, *Chem. Commun.* 51 (39) (2015) 8213–8228.
- [29] J. Wu, G.H. Ma, Recent studies of Pickering emulsions: Particles make the difference, *Small* 12 (2016) 4633–4648.
- [30] Z. Sun, X.X. Yan, Y. Xiao, L.J. Hu, M. Eggersdorfer, D. Chen, Z.Z. Yang, D.A. Weitz, Pickering emulsions stabilized by colloidal surfactants: Role of solid particles, *Particulology* 64 (2022) 153–163.
- [31] S. Peito, D. Peixoto, I. Ferreira-Faria, A.M. Martins, H.M. Ribeiro, F. Veiga, J. Marto, A.C. Paiva-Santos, Nano- and microparticle-stabilized Pickering emulsions designed for topical therapeutics and cosmetic applications, *Int. J. Pharm.* 615 (2022), 121455.
- [32] M. Shen, D.E. Resasco, Emulsions stabilized by carbon nanotube-silica nanohybrids, *Langmuir* 25 (18) (2009) 10843–10851.
- [33] L. Ni, C. Yu, Q.B. Wei, D.M. Liu, J.S. Qiu, Pickering emulsion catalysis: Interfacial chemistry, catalyst design, challenges, and perspectives, *Angew. Chem. Int. Ed.* 61 (2022) e202115885.
- [34] C.M. Vis, A.-E. Nieuwelin, B.M. Weckhuysen, P.C.A. Bruijnincx, Continuous flow Pickering emulsion catalysis in droplet microfluidics studied with *in situ* Raman microscopy, *Chem. Eur. J.* 26 (66) (2020) 15099–15102.
- [35] Y. Meng, W.X. Sun, H. Yang, W. Wang, N. Jin, Y.C. Zhao, X.L. Zhang, H.Y. Lu, Fine tuning of surface properties of SiO<sub>2</sub> nanoparticles for the regulation of Pickering emulsions, *Colloids Surf. A Physicochem. Eng. Asp.* 592 (2020), 124603.
- [36] W.X. Sun, X.L. Zhang, C.Q. Yao, Q.Q. Wang, N. Jin, H.Y. Lv, Y.C. Zhao, Hydrodynamic characterization of continuous flow of Pickering droplets with solid nanoparticles in microchannel reactors, *Chem. Eng. Sci.* 245 (2021), 116838.
- [37] H. Yang, T. Zhou, W. Zhang, A strategy for separating and recycling solid catalysts based on the pH-triggered Pickering-emulsion inversion, *Angew. Chem. Int. Ed.* 52 (29) (2013) 7455–7459.
- [38] S.C. Thickett, P.B. Zetterlund, Graphene oxide (GO) nanosheets as oil-in-water emulsion stabilizers: Influence of oil phase polarity, *J. Colloid Interface Sci.* 442 (2015) 67–74.
- [39] A.N. El-hoshyoudi, E.G. Zaki, S.M. Elsaed, Experimental and Monte Carlo simulation of palmitate-guar gum derivative as a novel flooding agent in the underground reservoir, *J. Mol. Liq.* 302 (2020), 112502.
- [40] C. Griffith, H. Daigle, On the shear stability of water-in-water Pickering emulsions stabilized with silica nanoparticles, *J. Colloid Interface Sci.* 532 (2018) 83–91.
- [41] B.P. Binks, C.P. Whitby, Silica particle-stabilized emulsions of silicone oil and water: Aspects of emulsification, *Langmuir* 20 (2004) 1130–1137.

- [42] S. Arditty, C.P. Whitby, B.P. Binks, V. Schmitt, F. Leal-Calderon, Some general features of limited coalescence in solid-stabilized emulsions, *Eur. Phys. J. E* 11 (3) (2003) 273–281.
- [43] M.K. Mulligan, J.P. Rothstein, Deformation and breakup of micro- and nanoparticle stabilized droplets in microfluidic extensional flows, *Langmuir* 27 (16) (2011) 9760–9768.
- [44] Y. Mei, G.X. Li, P. Moldenaers, R. Cardinaels, Dynamics of particle-covered droplets in shear flow: Unusual breakup and deformation hysteresis, *Soft Matter* 12 (2016) 9407–9412.
- [45] Q. Wei, C. Yu, X. Song, Y. Zhong, L. Ni, Y. Ren, W. Guo, J. Yu, J. Qiu, Recognition of water-induced effects toward enhanced interaction between catalyst and reactant in alcohol oxidation, *J. Am. Chem. Soc.* 143 (16) (2021) 6071–6078.
- [46] C. Yu, L. Fan, J. Yang, Y. Shan, J. Qiu, Phase-reversal emulsion catalysis with CNT-TiO<sub>2</sub> nanohybrids for the selective oxidation of benzyl alcohol, *Chem. Eur. J.* 19 (48) (2013) 16192–16195.
- [47] Y. Shan, C. Yu, J. Yang, Q. Dong, X. Fan, J. Qiu, Thermodynamically stable Pickering emulsion configured with carbon-nanotube-bridged nanosheet-shaped layered double hydroxide for selective oxidation of benzyl alcohol, *ACS Appl. Mater. Interfaces* 7 (22) (2015) 12203–12209.
- [48] Y. Zhang, M. Zhang, H. Yang, Tuning biphasic catalysis reaction with a Pickering emulsion strategy exemplified by selective hydrogenation of benzene, *ChemCatChem* 10 (22) (2018) 5224–5230.
- [49] P. Zhang, C.Q. Yao, H.Y. Ma, N. Jin, X.L. Zhang, H.Y. Lu, Y.C. Zhao, Dynamic changes in gas-liquid mass transfer during Taylor flow in long serpentine square microchannels, *Chem. Eng. Sci.* 182 (2018) 17–27.
- [50] K.A. Triplett, S.M. Ghiaasiaan, S.I. Abdel-Khalik, D.L. Sadowski, Gas-liquid two-phase flow in microchannels-Part I: Two-phase flow patterns, *Int. J. Multiph. Flow* 25 (3) (1999) 377–394.